

Optimization of a Savonius hydrokinetic turbine for performance improvement: A comprehensive analysis of immersion depth and rotation direction

Mafira Ayu Ramdhani and Il Hyoung Cho*

Department of Ocean System Engineering, Jeju National University, Jeju 63243, South Korea

(Received February 12 2024, Revised April 7, 2024, Accepted April 12, 2024)

Abstract. The turbine system converts the kinetic energy of water flow to electricity by rotating the rotor in a restricted waterway between the seabed and free surface. A turbine system's immersion depth and rotation direction are significantly critical in the turbine's performance along with the shape of the rotor. This study has investigated the hydrodynamic performance of the Savonius hydrokinetic turbine (SHT) according to the immersion depth and rotation direction using computational fluid dynamics (CFD) simulations. The instantaneous torque, torque coefficient, and power coefficients are calculated for the immersion ratios Z/D ranging [0.25, 3.0] and both clockwise (CW) and counterclockwise (CCW) rotations. A flow visualization around the rotor is shown to clarify the correlation between the turbine's performance and the flow field. The CFD simulations show that the CCW rotation produces a higher power at shallow immersion, while the CW rotation performs better at deeper immersion. The immersion ratio should be greater than the minimum of $Z/D=1.0$ to obtain the maximum power production regardless of the rotation direction.

Keywords: CFD; immersion depth; power coefficient; rotation direction; Savonius hydrokinetic turbine

1. Introduction

Ocean and tidal currents have numerous merits for power production. Tidal currents are highly predictable, while major ocean currents, such as the Gulf Stream and the Kuroshio Current, flow persistently as part of ocean circulation systems. Therefore, diverse energy conversion systems using ocean/tidal current energy have been developed (Bahaj 2013). The extraction process of ocean/tidal current energy is the same as the hydrokinetic energy conversion from the river or stream. The kinetic energy of flowing water is converted into mechanical energy through the rotation of the rotor, and then the generator that connects to the rotor shaft produces electricity. The amount of mechanical energy that can be transferred by the rotor is dependent on the water density, flow velocity, and projected area of the turbine system (Güney *et al.* 2010).

The Savonius turbine, which turns by the drag forces on the curved surface of the rotor in the moving fluid, can be utilized to extract the kinetic energy of ocean and tidal currents (Savonius 1931). This owes to its outstanding starting characteristics, simple geometry, and the ability to

*Corresponding author, Professor, E-mail: cho0904@jejunu.ac.kr

work regardless of flow direction. The Savonius turbine is commonly utilized as a drag-type rotor in wind and water flow for power production. However, due to the negative drag force created on the returning rotor, which opposes the turbine rotation, the operating efficiency of a Savonius turbine is low, resulting in its limited commercial-scale applicability (Maldar *et al.* 2020). Researchers have studied experimental and computational approaches to improve the performance of the Savonius turbine by investigating aspect ratio of the rotor, the number of rotors and stacking, rotor shape, adding deflector, and adjusting the separation gap between the rotors (Akwa *et al.* 2012, Sobczak 2018, Thiyagaraj *et al.* 2021, Ahmed *et al.* 2013) over years. The design of the rotor local shape, regarding the optimal separation gap (overlap ratio; OR and gap ratio; GR), has been explored in previous papers (Ushiyama and Nagai 1988, Kerikous and Thévenin 2019, Ramdhani *et al.* 2024), resulting in the maximum power coefficient being obtained at OR=0.15 and GR=0.03.

In practice, a horizontal-axis Savonius turbine is situated at the waterway confined by the seabed and free surface (Whelan *et al.* 2009). By physical insight, the Savonius hydrokinetic turbine should be as close to the free surface as possible to improve the energy conversion. However, if it is too close to the free surface, it will be disturbed by the free surface, causing the flow field to become unstable to reduce the energy extraction. The optimal immersed depth of a turbine below the free surface exists, and finding this value is crucial to enhancing its performance. The presence of the free surface and seabed can introduce blockage effects that may affect the power extracted from the flow (Zilic *et al.* 2020). The blockage ratio is defined as the swept area of the turbine divided by the cross-sectional area of the flow. The presence of the free surface also has an impact on the drop in free surface level affecting the torque on the rotor and downstream wake (Myers and Bahaj 2007).

This study aims to investigate the effect of the immersion depth and rotation direction on the performance of the Savonius hydrokinetic turbine. The CFD simulation based on a two-dimensional model is performed. The volume of fluid (VOF) method and realizable $k-\varepsilon$ turbulence model are adopted to simulate the flow field. In section 2, the key parameters affecting the performance of a Savonius turbine are introduced along with the numerical model used in this study. Section 3 demonstrates the mesh generation and computational domain setup. In section 4, the comparison between the present CFD results and Nakajima's experimental data (Nakajima *et al.* 2008) is performed and the effects of different immersion ratios and rotation directions (CW, CCW) on the performance of the Savonius turbine and the flow characteristics around the rotor are discussed. Finally, the conclusions are drawn in Section 5.

2. Key parameters and numerical model

The power coefficient (C_p) of a hydrokinetic turbine is defined as the ratio of the extracted power to the energy available in the flow. It can be expressed as

$$C_p = \frac{P_E}{P_I} = \frac{P_E}{0.5\rho AU^3} \quad (1)$$

where P_E is the mechanical power from the conversion system obtained by multiplying the torque Q (Nm) and the angular velocity ω (rad/s) of the rotor.

The torque coefficient (C_t) is also a key parameter in determining the performance of the Savonius turbine

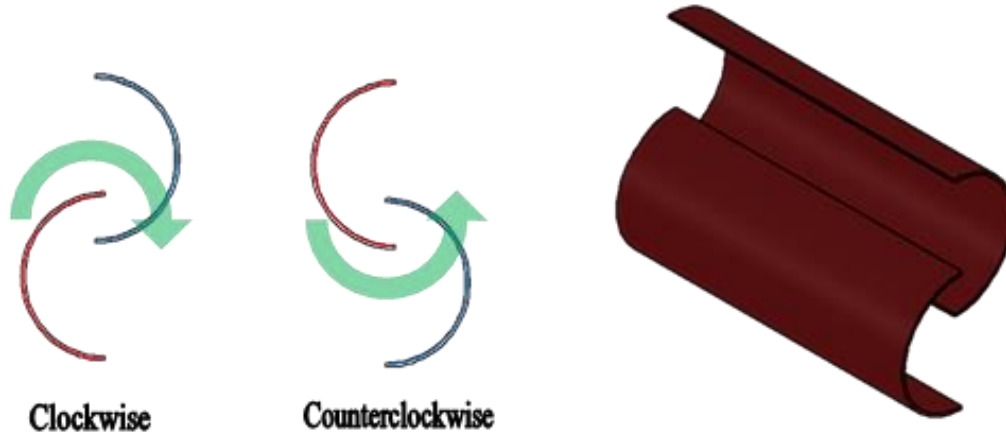


Fig. 1 Numerical model of the Savonius turbine with OR=0.15 and GR=-0.03

Table 1 Turbine specifications

Parameter	Value
Turbine length (L)	210 mm
Turbine diameter (D)	142 mm
Number of rotors	2
Rotor diameter (d)	89 mm
Overlap ratio (OR)	0.15
Gap ratio (GR)	-0.03

$$C_t = \frac{Q}{Q_t} = \frac{Q}{\frac{1}{2} \rho A U^2 R} \quad (2)$$

where A is the projected area of the turbine and R is the rotor's radius.

The power coefficient is closely dependent on the tip speed ratio (TSR), which is defined by the ratio of the tip speed of the rotor to the undisturbed current speed U . The TSR (λ) can be expressed as:

$$\lambda = \frac{\omega R}{U} \quad (3)$$

The specification for the Savonius turbine model shown in Fig. 1 is listed in Table 1. The overlap ratio (OR) and the gap ratio (GR) are key parameters affecting the rotor's performance. We use OR=0.15 and GR=-0.03, which are optimal values determined in the previous study (Ramdhani *et al.* 2024).

Both the clockwise (CW) and counterclockwise (CCW) of the rotor are considered in the numerical simulations. As indicated in Fig. 1, the blue color represents the advancing rotor, where the turbine absorbs kinetic energy, and the red color represents the returning rotor, where pressure is restored.

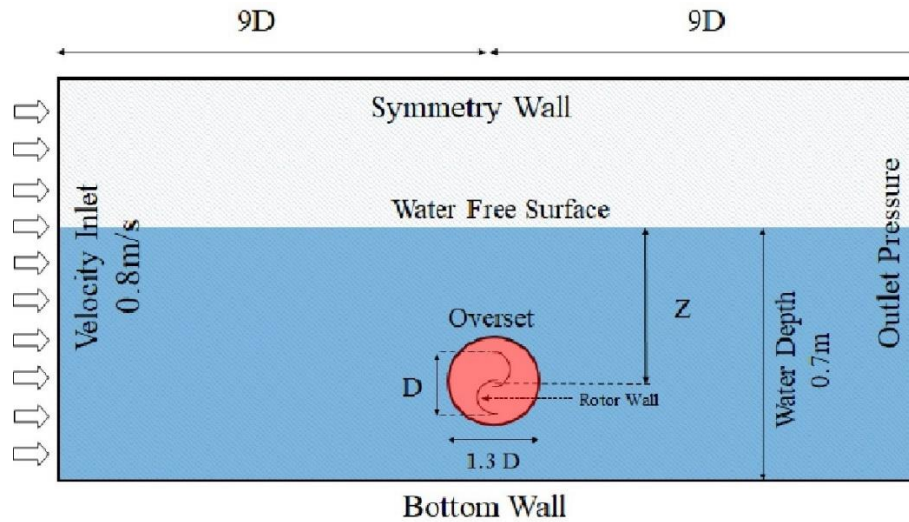


Fig. 2 Computational domain and boundary conditions

3. Computational methodology

In this study, Star-CCM+ CFD software is used to solve URANS (Unsteady Reynolds-averaged Navier-Stokes) equations. For simplicity, the present numerical model is assumed to be a two-dimensional model. A finite volume method (FVM), which is a well-established computational approach, has been employed. This method is utilized to discretize the fluid domain and solve the governing equations within the discretized numerical domain (Tu *et al.* 2008). The Volume of Fluid (VOF) method is adopted to track the free surface between water and air (Hirt and Nichols 1981). The realizable k - ϵ turbulence model was used to model the turbulence in the flow as it is well suited for simulating flow around the rotating machinery compared to the standard version (Shih *et al.* 1995).

To precisely capture the rotating motion of the Savonius rotor, the overset mesh technique was implemented. This approach is well known to yield faster convergence and superior accuracy in comparison to the sliding mesh technique (Lopez *et al.* 2021). To implement the overset mesh technique, the entire fluid domain is divided into two distinct sub-domains: a rotating domain, which rotates together with the rotor, and a stationary domain which represents the flow of water (UniAET 2020). The overset boundary positioned between them plays a crucial role in facilitating the seamless transfer of mesh data between the rotating and stationary domains. It is worth noting that our numerical simulations are conducted in an unsteady state, allowing us to capture the rate of dynamic changes over time.

The whole fluid domain is $18D$ in length (D is a turbine diameter). The distance between the rotor and inlet boundary is $9D$, and the distance from the center of the turbine to the upper and lower boundaries is dependent on the immersion ratio ($Z^*=Z/D$). The immersion ratio is the distance between the free surface and the center of the turbine divided by the turbine diameter. In all the cases, the water depth is fixed to be 0.7 m . The size of the overset domain is $1.3D$, 30% larger than the rotor diameter.

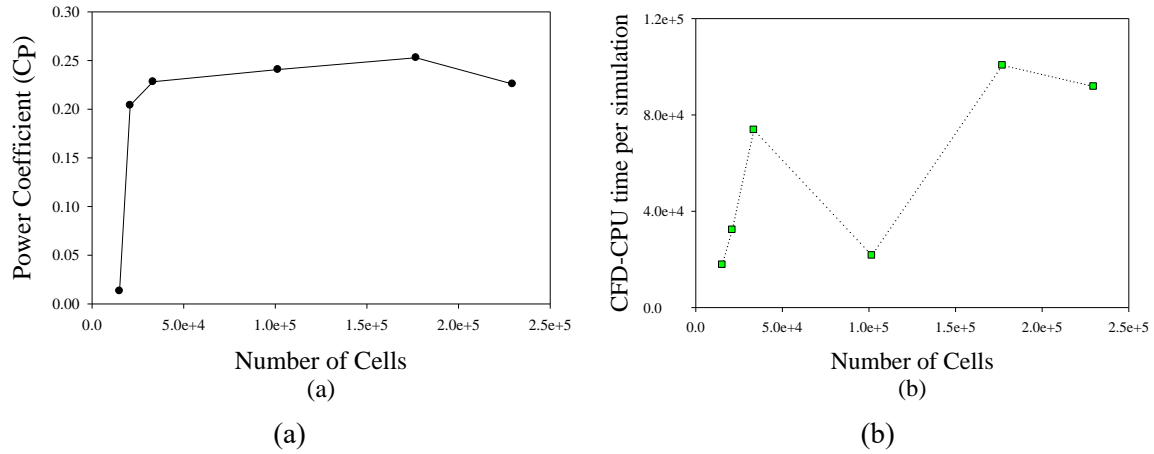


Fig. 3 (a) grid independence test and (b) CFD-CPU time convergence

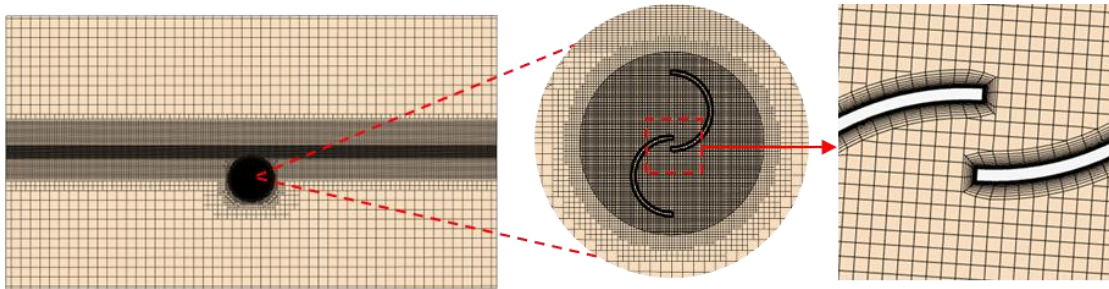


Fig. 4 Mesh distribution in numerical domain

At the inlet boundary, a uniform current velocity of 0.8 m/s is prescribed. The pressure outlet condition is applied at the outlet boundary to consider the back-flow due to the rotating turbine. The symmetry condition is imposed at the top wall to represent the infinite air domain. The bottom boundary is treated as a wall to express the seabed. A no-slip condition is enforced along the surface of the rotor. The computational domain and boundary conditions are depicted in Fig. 2.

A high-quality mesh is necessary to offer accurate, stable, and convergent numerical solutions; hence, mesh development is a vital step in conducting precise and efficient CFD calculations for a particular numerical model (Boissonnat *et al.* 2006). Therefore, it is necessary to evaluate the suitability of mesh resolution before conducting any numerical studies. A fine mesh is used near the rotor and free surface. Additionally, the mesh size in the stationary region gradually increases away from the free surface. The grid convergence test is carried out by comparing the power performance for six different mesh counts, ranging from coarse to fine mesh with combination of various prism layers (Almohammadi *et al.* 2012). In Fig. 3(b), we observe that the CPU time generally increases as the number of cells increases. However, at a cell count of 1×10^5 , the CPU time drastically reduces, which is affected by the change in the number of prism layers and the first cell thickness. A mesh count of 1×10^5 was applied considering the CPU time, storage, and accuracy, seen in Fig. 3.

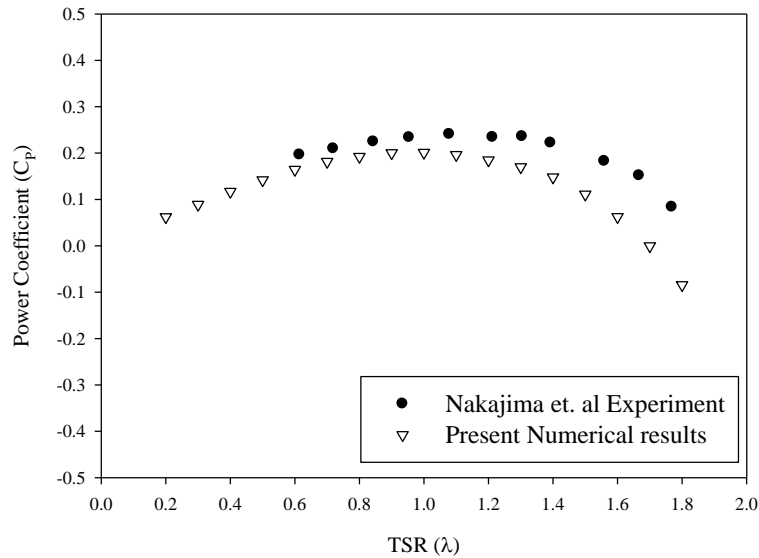


Fig. 5 Comparison of the power coefficient between the CFD results and Nakajima's experiments

From the grid independence result, in the present CFD simulation, we used a 2D automated mesh creation technique with a trimmed cell meshing model. We specifically put 15 prism layer cells surrounding the rotor. This intentional positioning of prism layer cells improves boundary layer resolution, which contributes to enhancing the simulation's overall accuracy (Ito and Nakahashi 2004, Almohammadi *et al.* 2012). The prism layer's distance from the rotor wall is managed to keep the non-dimensional wall distance (y^+) value below one. The local mesh surrounding the rotor and at the wall boundaries of the rotor are shown in Fig. 4.

4. Result and discussion

4.1 CFD validation

To confirm the CFD model's reliability, the numerical results are compared with the experimental data of Nakajima *et al.* (2008). Herein, the average power coefficient (C_p) is taken as the output for the comparison with the experiment. In Fig. 5, although discrepancy appears at the large TSR, the average power coefficient shows a satisfactory agreement within the overall range [0.2, 1.8] of TSR. The discrepancy may occur due to the dimensionality effect, which should take into consideration the effect of the end plate and aspect ratio to fully represent the experimental result. Besides, the underestimation of C_p and the error may happen due to the chaotic flow distribution around the turbine at higher TSR, as similarly reported in the previous study. (Roy and Saha 2013, Satrio *et al.* 2018, Chemengich *et al.* 2022). Given the established reliability of the present CFD model, it will be utilized to conduct a parametric study to determine the optimal immersion depth and rotation direction of a Savonius rotor.

Table 2 Key parameters for CFD simulation

Rotation direction	Immersion ratio (Z/D)
Clockwise (CW)	0.25, 0.50, 0.75, 1.00, 1.50, 2.00, 2.50, 3.00
Counterclockwise (CCW)	

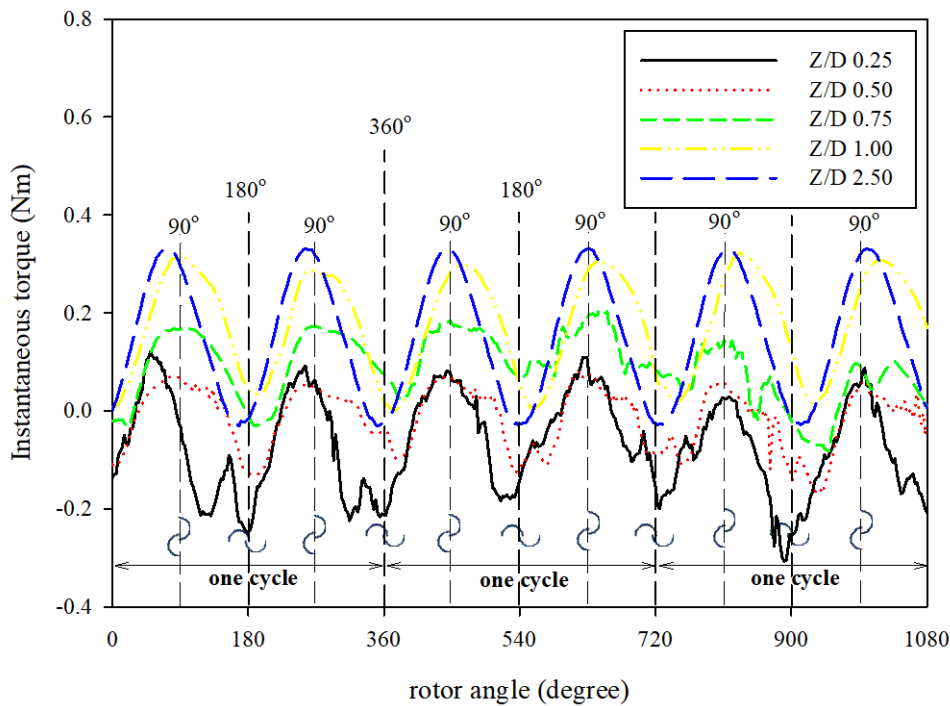


Fig. 6 Instantaneous torques of the CW rotating turbine for different immersion ratios at TSR=0.8

4.2 Turbine performance

The torque, torque coefficient, and power coefficient of the Savonius hydrokinetic turbine are calculated to investigate the effect of the free surface on its performance. The simulation was carried out following the conditions shown in Table 2. The immersion ratio used in this study ranges from 0.25 to 3.0.

4.2.1 Clockwise (CW) rotation

Fig. 6 depicts the time series of instantaneous torque versus the rotation angle of the rotor for five different immersion ratios at a fixed TSR of 0.8 when rotating in CW. The torque reaches the peak twice within one cycle due to the characteristics of two-cup-shaped rotors adopted in the present study. As seen in the figure, the instantaneous torque of a turbine with an immersion ratio larger than 1.0 gives a higher torque with reduced influence by the free surface. It also shows that

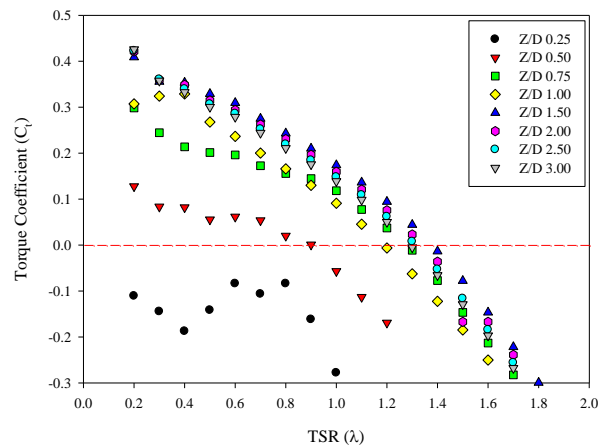


Fig. 7 Average torque coefficient of the CW-rotating turbine as a function of immersion ratio and TSR

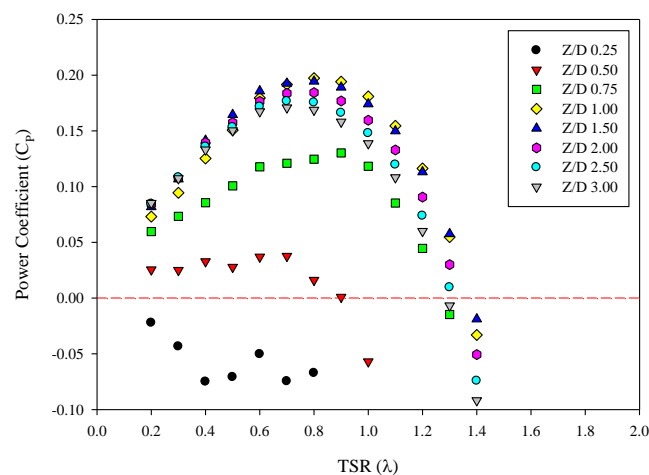


Fig. 8 Average power coefficient of the CW-rotating turbine as a function of immersion ratio and TSR

with the rotor placed far away from the free surface, the torque follows the smooth sinusoidal curve. However, as the turbine is positioned closer to the free surface, the torque curve is distorted severely due to the effect of the free surface.

The average torque coefficient (C_t) versus TSR is shown in Fig. 7. It shows that as the turbine is closer to the free surface, C_t has a lower value. Regardless of the immersion ratio, the torque coefficient tends to decrease as the TSR increases. When the immersion ratio Z/D is greater than 1.0, the differences in each torque coefficient are insignificant. This indicates that the influence of the free surface can be disregarded at $Z/D \geq 1.0$. The overall curve of torque coefficient at shallow immersion of $Z/D=0.25$ drops below 0, which depicts that the situation is unsuitable for energy generation.

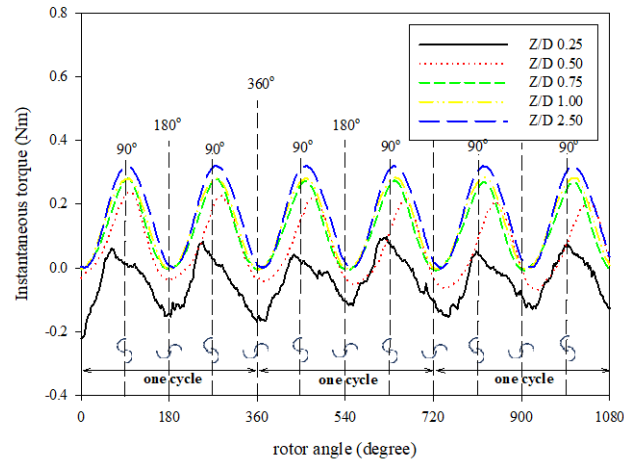


Fig. 9 Instantaneous torques of the CCW rotating turbine for different immersion ratios at TSR=0.7

When the turbine is rotating CW, the effect of immersion ratio on the power coefficient (C_p) is shown in Fig. 8. As seen in the figure, the curve of C_p shows the peak values around TSR=0.8 when Z/D is greater than 1.0. The power coefficient has a maximum power coefficient of $C_p=0.197$ at TSR=0.8 and $Z/D=1.0$. After reaching its peak, the power coefficient declines with an increase in TSR. In the case of the shallow immersion with $Z/D=0.25$, C_p drops even below 0.0 within an entire range of TSR and its pattern is unpredictable.

4.2.2 Counterclockwise (CCW) rotation

This paper further investigates the impact of the immersion ratio on the counterclockwise rotating Savonius turbine. The instantaneous torque for five different immersion ratios is shown in Fig. 9. Contrary to other immersion ratios, the instantaneous torque of $Z/D=0.25$ is located below the zero-torque line. Fig. 9 shows that the Savonius hydrokinetic turbine with CCW rotation exhibits a smoother and slightly higher instantaneous torque than the CW-rotating turbine in Fig. 6.

According to Fig. 10, the average torque coefficient (C_t) decreases as TSR increases, and C_t values are too low and cannot be used in the energy converter when TSR is greater than 1.1. Fig. 10 also demonstrates how the torque coefficient increases as the immersion ratio increases. Excluding $Z/D=0.25$, the curves of C_t show a similar trend regardless of the immersion ratio. Deployment of the turbine system too close to the free surface makes power production difficult, as proved in $Z/D=0.25$. A similar finding has been reported for the CCW-rotating turbine by Zhang *et al.* (2024)

Fig. 11 shows the average power coefficient versus TSR under different immersion ratios. As seen in Fig. 11, the C_p curve reaches its peak at the TSR=0.7 and $Z/D=1.0$. However, when the immersion ratios are below 1.0, the peak occurs at the lower TSR. As previously mentioned, the increase in immersion depth of the turbine enhances the power coefficient. The maximum power coefficient of $C_{pmax}=0.17$ is generated at $Z/D=3.0$, and TSR=0.7. Moreover, Fig. 11 shows that the power coefficient rapidly drops at the transition from $Z/D=0.50$ to $Z/D=0.25$. In the majority of

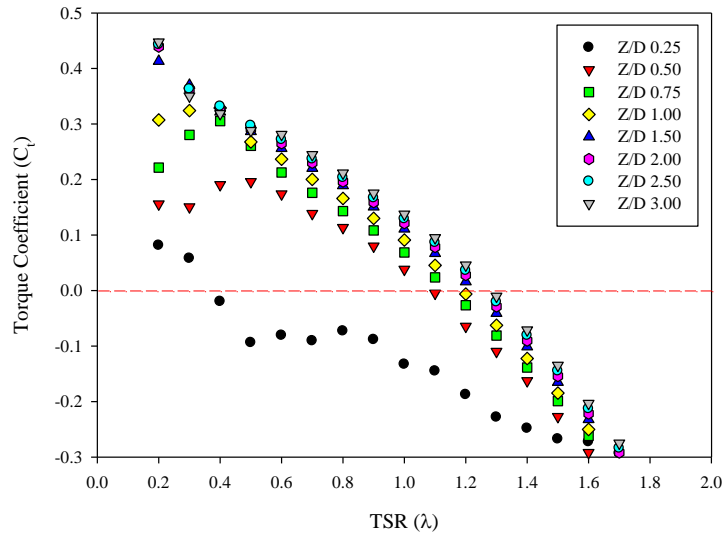


Fig. 10 Average torque coefficient of the CCW rotating turbine as a function of immersion ratio and TSR

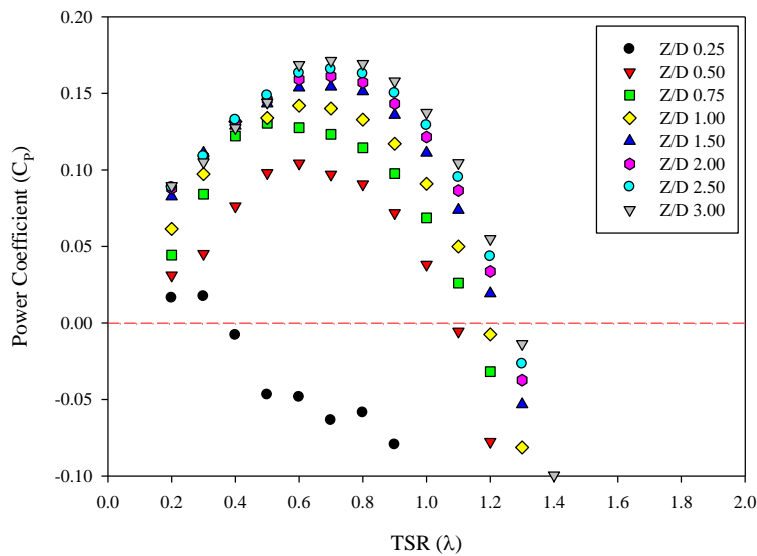


Fig. 11 Average power coefficient of the CCW-rotating turbine as a function of immersion ratio and TSR

immersion ratios except for $Z/D=0.25$, the curves of the power coefficient followed a similar trend: reaching its maximum and then decreasing as TSR increases. In comparing CW- and CCW rotating, the CW-rotating shows a higher power coefficient, however, at $Z/D=0.50$, the reverse tendency is identified.

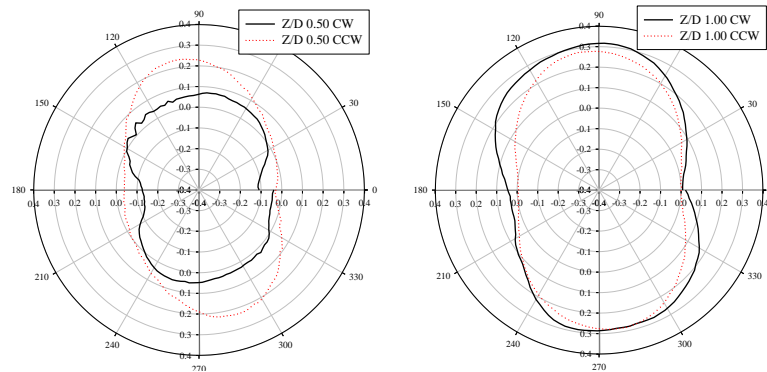


Fig. 12 Polar plot of instantaneous torque for the CW- and CCW- rotating turbine at $Z/D=0.50$ and $Z/D=1.00$

Fig. 12 represents the polar plots of instantaneous torque at $Z/D=0.5$ and 1.0 for two different rotation directions (CW, CCW). Fig. 12 demonstrates that the deeper submerged turbine shows a larger torque. At $Z/D=0.5$, the area of instantaneous torque on CCW rotation is larger than CW rotation, however, at $Z/D=1.0$ the CW-rotating turbine yields a slightly higher value of instantaneous torque than CCW rotation. In addition, the vertical instant attitude of the turbine representing the rotation angle of 90° and 270° gives a higher torque than the horizontal instant attitude with 0° and 180° .

4.3 Flow visualization around turbine

To clarify the flow characteristics around the turbine, flow visualization is drawn in Fig. 13 for two different immersion ratios, $Z/D=0.50$ and $Z/D=1.00$ for the CW-rotating turbine. $TSR=0.8$ is used, which corresponds to an optimal value giving C_{Pmax} . At $Z/D=0.50$, the rotation center is on the free surface, while the turbine is fully submerged at $Z/D=1.0$. The snapshots of the free-surface deformation and flow velocity are shown in four successive rotation angles of 0° , 45° , 90° , and 135° within one cycle. The direction of water flow is the positive x-axis.

As shown in Fig. 13, the magnitude of flow velocity downstream of the turbine is visible between two immersion ratios. The zone of a low velocity is observed downstream at $Z/D=0.5$, however, a similar region does not exist in the wake region at $Z/D=1.0$. On the contrary, at $Z/D=1.0$, a higher velocity zone around the concave surface of the returning rotor is shown, and the appearance of wake vortex and overlap vortex is more pronounced, compared to a lower immersion ratio $Z/D=0.5$. When the rotation direction of the rotor coincides with the flow direction of water, the increased drag force and pressure restoration effect increase the turbine's performance.

As mentioned earlier, the presence of a turbine in flowing water can stimulate the deformation of the free surface and wake formation. Comparing two immersion ratios, at $\theta = 135^\circ$, the free surface level at $Z/D=1.0$ drops up to 10 cm lower than the still water level. The drop in the free surface level observed by Whelan *et al.* (2009), accelerates air and water to be mixed. This trapped air in the water surrounding the turbines can potentially hinder their performance by diminishing the kinetic energy absorbed by the rotor. Such performance degradation of the turbine was reported by Birjandi *et al.* (2013).

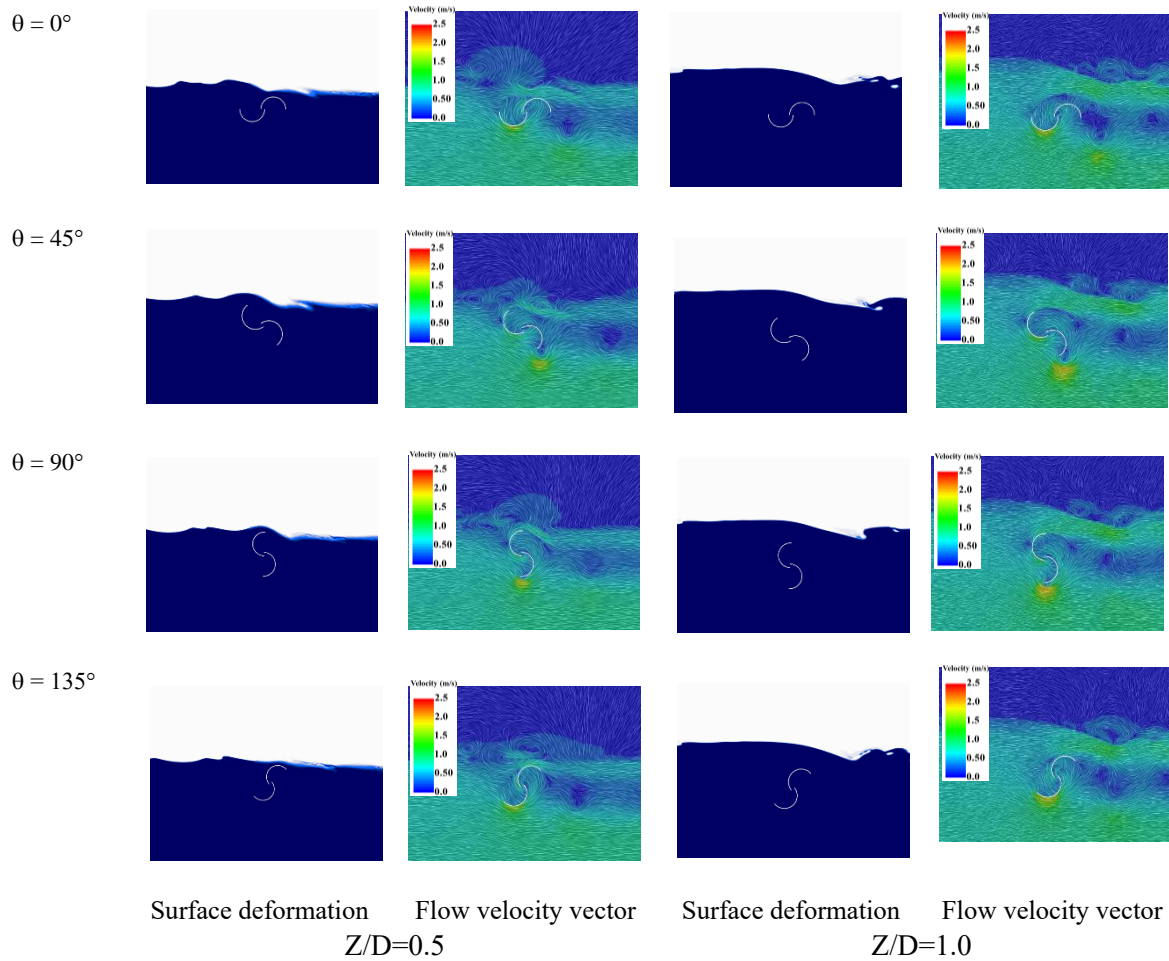


Fig. 14 Free-surface deformation and flow velocity vector around the CCW-rotating turbine

To estimate the overall performance of the Savonius torque for two key parameters such as immersion ratio and rotation direction, the power coefficient is drawn as a function of TSR and immersion ratio, in Fig. 16. At $Z/D=0.5$, the power coefficient shows a significant difference between CW- and CCW- rotating turbines. At deeper immersion of $Z/D=1.0$, better performance is identified. It also shows that the performance of the CW-rotating turbine is superior to CCW rotation, contrary to $Z/D=0.5$

5. Conclusions

In this study, a comprehensive study on the effect of the immersion ratio (Z/D) and rotation direction (CW, CCW) was performed on the Savonius hydrokinetic turbine. The CFD numerical method was used to simulate the behavior of the Savonius hydrokinetic turbine in water flow. To

verify the present CFD model, the CFD results were compared with the experimental data. From a series of CFD simulations, several key conclusions have been drawn:

1. The performance of the Savonius hydrokinetic turbine is significantly affected by the immersion ratio and rotation direction. The CFD results show that the effect of the free surface diminishes with increasing immersion depth and the torque coefficient generally decreases with an increase of TSR. Interestingly, the shallow immersion of a turbine of $Z/D=0.25$ proves impracticality for energy generation due to negative instantaneous torque.
2. $C_{P_{max}}$ is higher relatively when the turbine rotates in CCW for $Z/D < 0.50$. However, after the bifurcation point of $Z/D=0.75$, the CW-rotating turbine is superior to the rotation in CCW. In the CW-rotating, the maximum power coefficient is $C_{P_{max}}=0.197$ at $TSR=0.8$ and $Z/D=1.0$. On the other hand, in the CCW rotation, the maximum power coefficient of 0.17 is generated at $Z/D=3.0$ and $TSR=0.7$.
3. The visualization of flow filed around a rotating turbine at $Z/D=0.50$ and $Z/D=1.00$, considering both the CW- and CCW-rotation, unveils crucial insights. The CW-rotating turbine at $Z/D=1.0$ creates a zone of a higher velocity around the tip of the advancing rotor, consequently increasing turbine performance. However, air trapping in water generated at $Z/D=0.5$ detains kinetic energy absorption. In contrast to the CW-rotating turbine, the flow around the CCW-rotating turbine shows similar flow characteristics regardless of immersion ratio.
4. Rotating direction plays a crucial role, with the counterclockwise (CCW) rotation showing a higher $C_{P_{max}}$ value at shallow immersion ratios ($Z/D < 0.75$), while the clockwise (CW) rotating turbine performs better at deeper immersions ($Z/D \geq 1.00$).

Acknowledgments

The researcher uses this opportunity to express our appreciation to NIIED (National Institute for International Education) sponsored by Korean Ministry of Education.

References

- Ahmed, Y., Hassanzadeh, R., Yaakob, O. and Ismail, M. (2013), "Comparison of conventional and helical Savonius marine current turbine using computational fluid dynamics", *World Appl. Sci. J.*, **28**, 1113-1119.
- Akwa, J.V., Vielmo, H.A. and Petry, A.P. (2012), "A review on the performance of Savonius wind turbines", *Renew. Sust. Energ. Rev.*, **16**(5), 3054-3064. <https://doi.org/10.1016/j.rser.2012.02.056>.
- Almohammadi, K.M., Ingham, D.B. and Ma, L. (2012), "Pourkashanian M. CFD sensitivity analysis of a straight-blade vertical axis wind turbine", *Wind Eng.*, **36**(5), 571-588. <https://doi.org/10.1260/0309-524X.36.5>.
- Almohammadi, K.M., Ingham, D.B., Ma, L. and Pourkashan, M. (2013), "Computational fluid dynamics (CFD) mesh independency techniques for a straight blade vertical axis wind turbine", *Energy*, **58**, 483-493. <https://doi.org/10.1016/j.energy.2013.06.012>.
- Bahaj, A.S. (2013), "Marine current energy conversion: The dawn of a new era in electricity production", *Philos. T. R. Soc. A.*, **371**, 20120500. <https://doi.org/10.1098/rsta.2012.0500>.
- Birjandi, A.H., Bibeau, E.L., Chatoorgoon, V. and Kumar, A. (2013), "Power measurement of hydrokinetic turbines with free-surface and blockage effect", *Ocean Eng.*, **69**, 9-17. <https://doi.org/10.1016/j.oceaneng.2013.05.023>.

- Boissonnat, J.D., Cohen-Steiner, D., Mourrain, B., Rote, G. and Vegter, G. (2006), "Meshing of Surfaces". In: Boissonnat, J.D. and Teillaud, M. (Eds), *Effective computational geometry for curves and surfaces*. Springer, Berlin, Heidelberg.
- Chemengich, S.J., Kassab, S.Z. and Lotfy, E.R. (2022), "Effect of the variations of the gap flow guides geometry on the savonius wind turbine performance: 2D and 3D studies", *J. Wind Eng. Ind. Aerod.*, **222**, 104920. <https://doi.org/10.1016/j.jweia.2022.104920>.
- Güney, M.S. and Kaygusuz, K. (2010), "Hydrokinetic energy conversion systems: A technology status review", *Renew. Sust. Energ. Rev.*, **14**(9), 2996-3004. <https://doi.org/10.1016/j.rser.2010.06.016>.
- Hirt, C.W. and Nichols, B.D. (1981), "Volume of Fluid (VOF) method for the dynamics of free boundaries", *J. Comput. Phys.*, **39**(1), 201. [https://doi.org/10.1016/0021-9991\(81\)90145-5](https://doi.org/10.1016/0021-9991(81)90145-5).
- Ito, Y. and Nakahashi, K. (2004), "Improvements in the reliability and quality of unstructured hybrid mesh generation", *Int. J. Numer. Meth. Fl.*, **45**(1), 79-108. <https://doi.org/10.1002/flid.669>.
- Kerikous, E. and Thévenin, D. (2019), "Performance enhancement of a hydraulic Savonius turbine by optimizing overlap and gap ratios", *Proceedings of the ASME 2019 Gas Turbine India Conference*, Chennai, India.
- Mejia, O.D.L., Mejia, O.E., Escorcía, K.M., Suarez, F. and Laín, S. (2021), "Comparison of sliding and overset mesh techniques in the simulation of a vertical axis turbine for hydrokinetic applications", *Processes*, **9**(11), 1933. <https://doi.org/10.3390/pr9111933>.
- Maldar, N.R., Ng, C.Y. and Oguz, E. (2020), "A review of the optimization studies for Savonius turbine considering hydrokinetic applications", *Energ. Convers. Management*, **226**, 113495. <https://doi.org/10.1016/j.enconman.2020.113495>.
- Myers, L. and Bahaj, A.S. (2007), "Wake studies of a 1/30th scale horizontal axis marine current turbine", *Ocean Eng.*, **34**(5-6), 758-762. <https://doi.org/10.1016/j.oceaneng.2006.04.013>.
- Nakajima, M., Iio, S. and Ikeda, T. (2008), "Performance of Savonius rotor for environmentally friendly hydraulic turbine", *J. Fluid Sci. Tech.*, **3**, 420-429. <https://doi.org/10.1299/jfst.3.420>.
- Ramdhani, M.A., George, A. and Cho, I.H. (2024), "Influence of separation gap on the performance of Savonius hydrokinetic turbine", *Intel. Sustain. Manufact.*, **1**(1), 10005. <https://doi.org/10.35534/ism.2024.10005>.
- Roy, S. and Saha, U.K., (2013), "Review on the numerical investigations into the design and development of Savonius wind rotors", *Renew. Sust. Energ. Rev.*, **24**, 73-83. <https://doi.org/10.1016/j.rser.2013.03.060>.
- Satrio, D., Utama, I.K. and Mukhtasor, M., (2018), "The influence of time step setting on the CFD simulation result of vertical axis tidal current turbine", *J. Mech. Eng. Sci.*, **12**(1), 3399-3409. <https://doi.org/10.15282/jmes.12.1.2018.9.0303>.
- Savonius, S.J. (1931), "The S-rotor and its applications", *Mech. Eng.*, **53**, 333-338.
- Shih, T.H., Liou, W.W., Shabbir, A., Yang, Z. and Zhu, J. (1995), "A new k- ϵ eddy viscosity model for high Reynolds number turbulent flows", *Comput. Fluids*, **24**(3), 227-238. [https://doi.org/10.1016/0045-7930\(94\)00032-T](https://doi.org/10.1016/0045-7930(94)00032-T).
- Sobczak, K. (2018), "Numerical investigations of an influence of the aspect ratio on the Savonius rotor performance", *J. Phys.: Conf. Ser.*, **1101**, 012034. <https://doi.org/10.1088/1742-6596/1101/1/012034>.
- Thiyagaraj, J., Rahamathullah, I., Anbuhezhiyan, G., Barathiraja, R. and Ponshanmugakumar, A. (2021), "Influence of blade numbers, overlap ratio and modified blades on performance characteristics of the savonius hydro-kinetic turbine", *Materials Today: Proceedings*, **46**(9), 4047-4053. <https://doi.org/10.1016/j.matpr.2021.02.568>.
- Tu, J., Yeoh, G.H. and Liu, C. (2008), "Computational fluid dynamics-a practical approach", Butterworth-Heinemann: Oxford, UK.
- UniAET (2020), "Simcenter STAR-CCM+ Basic Training", Siemens: Munich, Germany.
- Ushiyama, I. and Nagai, H. (1988), "Optimum design configurations and performance of Savonius rotors", *Wind Eng.*, **12**(1), 59-75.
- Whelan, J.I., Graham, J.M.R. and Perio, J. (2009), "A free-surface and blockage correction for tidal turbines", *J. Fluid Mech.*, **624**, 281-291. <https://doi.org/10.1017/S0022112009005916>.

- Zhang, B., Li, B., Li, C., Zhang, Y., Lv, J. and Yu, H. (2024), "Effects of submergence depth on the performance of the Savonius hydrokinetic turbine near a free surface", *Energy*, **289**, 129899. <https://doi.org/10.1016/j.energy.2023.129899>
- Zilic de Arcos, F., Tampier, G., and Vogel, C.R. (2020), "Numerical analysis of blockage correction methods for tidal turbines", *J. Ocean Eng. Mar. Energy*, **6**, 183-197. <https://doi.org/10.1007/s40722-020-00168-6>.

PL